ACS Macro Letters

Letter

pubs.acs.org/macroletters

Glass-Transition and Side-Chain Dynamics in Thin Films: Explaining Dissimilar Free Surface Effects for Polystyrene vs Poly(methyl methacrylate)

David D. Hsu,[†,∥] Wenjie Xia,[‡,∥] Jake Song,[§] and Sinan Keten*[,†,‡]

[†]Department of Mechanical Engineering, [‡]Department of Civil & Environmental Engineering, and [§]Department of Materials Science & Engineering, Northwestern University, 2145 Sheridan Road, Evanston, Illinois 60208-3109, United States

Supporting Information

ABSTRACT: Despite having very similar bulk properties such as glass-transition temperature (T_g), density, and fragility, polystyrene (PS) and poly(methyl methacrylate) (PMMA) exhibit characteristically different T_g depression in free-standing ultrathin films due to free surface effects. Here we explain this difference using our recently established chemistry-specific coarse-grained (CG) models for these two polymers. Models capture the dissimilar scaling of T_g with free-standing film thickness as seen in experiments and enable us to quantify the size of the regions near free surfaces over which chain relaxation exhibits differences from bulk. Most interestingly, vibrational density of states (VDOS) analysis uncovers a relationship between the amplitude of side-chain fluctuations, associated with side-chain flexibility and T_g-nanoconfinement. We discover that increasing backbone to side-chain mass ratio in CG models increases the amplitude of side-chain fluctuations and suppresses the free-surface effect on T_g. We show that mass distribution and side-chain flexibility are central to explain dissimilar free surface effects on PS and PMMA. Our model predictions are further corroborated by experimental evidence showing the role of mass distribution in styrene thin films. Our study ascertains the significance of molecular characteristics on nanoconfinement and highlights the ability for chemistry-specific CG models to explore the thermomechanical properties of polymer thin films.

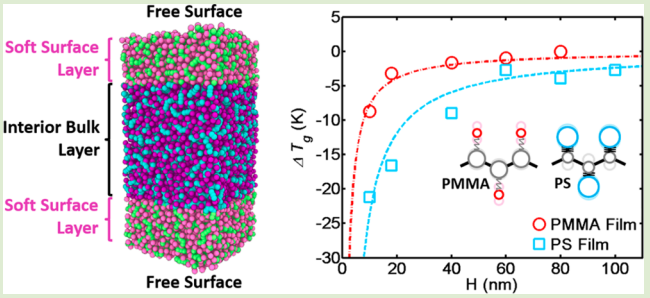

Glass-transition and structural relaxation in polymer thin films with nanoscale thicknesses significantly deviate from known bulk behavior of constituent polymers. This effect, broadly referred to as the nanoconfinement effect, occurs due to the presence of polymer−air or polymer−substrate interfaces in films, where the discontinuity in the neighboring interactions of polymer chains near the free surface or solid substrate influences a large portion of nanoscale films by volume. This can cause large shifts in key material properties such as the glass-transition temperature (T_g),[1−6] relaxation dynamics,[7−10] and mechanical properties.[11−14] In freely standing thin films, T_g reduces with decreasing film thickness due to a "liquid-like" surface layer stemming from the reduction of topological constraints at the free surfaces.[1,15,16] This portrayal, however, lacks an explanation as for why some polymers undergo greater T_g reduction than others. Toward this effort, many hypotheses have been proposed to explain unique experimental observations, but none provide a comprehensive narrative.

An observation that remains particularly challenging is the dissimilar T_g behaviors between poly(styrene) (PS) and poly(methyl methacrylate) (PMMA) in free-standing thin films. PS and PMMA display remarkable similarities in bulk properties, such as bulk T_g, density, elastic properties, persistence length, surface tension, and fragility (see Table 1), but surprisingly have characteristically different T_g depression in the film configuration.[22,23] Roth et al. studied free-standing film T_g through transmission ellipsometry and found that at a film thickness of 40 nm, PS (M_w = 767 × 10^3 g/mol), exhibits a T_g reduction of 52 K compared to 15 K for PMMA (M_w = 790 × 10^3 g/mol).[17,22] Systematic modifications to PS and PMMA have also been performed to explore trends pertinent to the free-surface effect such as length scale of cooperative segmental dynamics ξ (CRR),[24−26] backbone rigidity,[25,27] side-chain flexibility,[26,28] and fragility.[29,30] However, in comparing PS vs. PMMA, a mechanistic explanation for the strength of free-surface-induced T_g reductions as a result of chemical structure remains unclear. In the present study, to explore the T_g-confinement behaviors of free-standing films, we employ coarse-grained (CG) models derived from our recently developed thermomechanically consistent coarse-graining method (TCCG)[31,32] (Figure 1). By using vibrational density of states analysis (VDOS) and systematically varying parameters in the CG models, we are able to uncover underlying mechanisms of T_g-confinement effect differences as observed in PS and PMMA free-standing films. To our best knowledge, this work presents the first bottom-up approach

Received: January 19, 2016
Accepted: March 14, 2016
Published: March 29, 2016

DOI: 10.1021/acsmacrolett.6b00037
ACS Macro Lett. 2016, 5, 481−486

Table 1. Bulk Experimental Properties for PS and PMMA

type	monomer weight (g/mol)	bulk $T_{g\infty}$ (K)	ρ^a (g/cm^3)	modulus^a (GPa)	fragility m	$C_\infty{}^a$
PS	104.15	370[17]	1.04[18]	2.3−3.3[18]	118−142[19]	9.85[20]
PMMA	100.12	385[17]	1.10[18]	2.2−3.8[18]	103−145[19]	9.0[21]

[a]At 300 K.

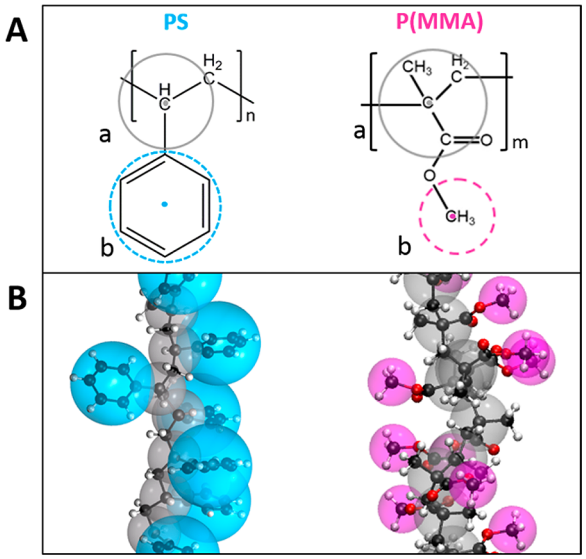

Figure 1. (A) Polymer structure and coarse-grained bead force center locations of backbone (a) and side-chain beads (b) for PS and PMMA. (B) Two-bead per monomer coarse-grained bead model shown overlaid on the all-atomistic system.

with molecular resolution toward explaining the T_g-nano-confinement differences between PS and PMMA free-standing thin films.

To characterize confinement differences between PS and PMMA CG models, we first calculate and compare α-relaxation times τ_α as a function of temperature for the bulk and ∼18 nm thick film systems (Figure 2a). The methodology we use to calculate τ_α and T_g from the dynamic structure factor relaxation is described in detail in the Supporting Information. Our analysis reveals that Vogel−Fulcher−Tammann (VFT) curves for PS exhibit a greater shift than PMMA between bulk and 18 nm film at the relaxation time associated with computational T_g, estimated at the temperature where τ_α = 1 ns.[33−35] ΔT_g (= $T_g^{film} - T_g^{bulk}$) is a measure of the degree of confinement and is found to be −17 and −3 K for PS and PMMA, respectively, at ∼18 nm film thickness. In addition, PS exhibits a larger depression of the film T_g with decreasing thickness H than PMMA (Figure 2b), indicating a greater enhancement in chain mobility and relaxation dynamics induced by the free surface for the PS film. ΔT_g vs thickness data are fitted with the empirical function:[4] $T_g(H) = T_g^{bulk}[1 - (A/H)^\delta]$, where A and δ are fitting constants. At $H \approx 40$ nm, the PMMA film T_g converges to the bulk value, whereas the T_g convergence for PS occurs at a greater thickness $H \approx 100$ nm. Experimental measurements tend to indicate a higher degree of depression than estimated by the incumbent simulations. This is likely because T_g is calculated at higher cooling rates in simulations, which can suppress the mobility gradient.[36,37] Despite this difference, we find that our simulation results remain in significant qualitative agreement with experiments and are also consistent with other computational studies.[38] Our CG models are derived using a consistent approach and have been tuned to

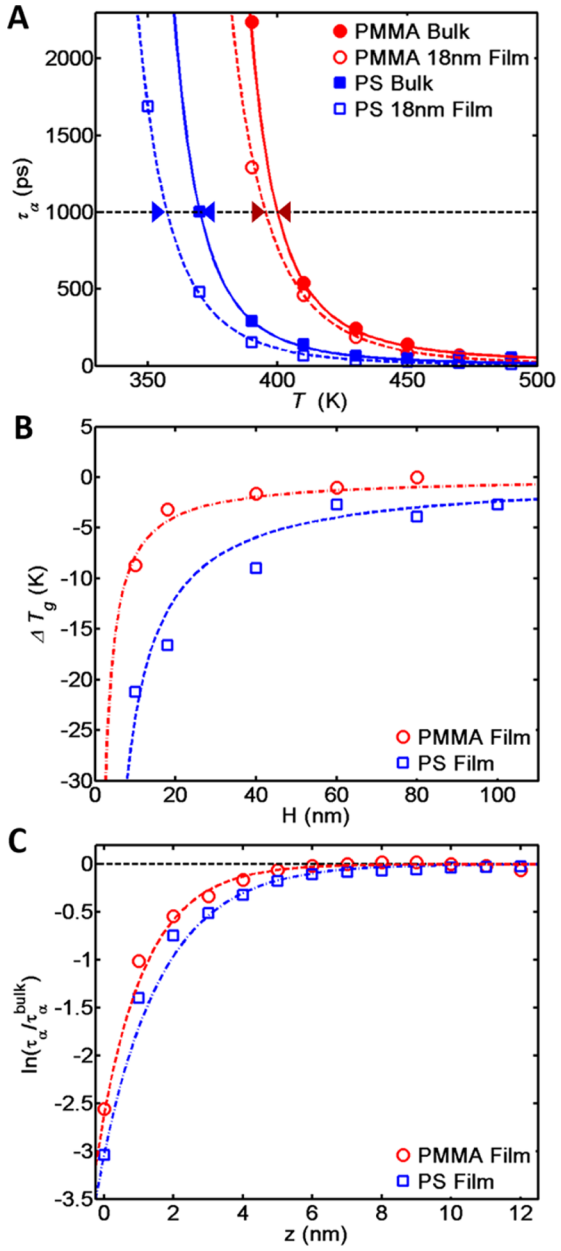

Figure 2. (A) Vogel−Fulcher−Tammann (VFT) fit of temperature-dependent α-relaxation times. PMMA bulk and 18 nm film data shown as filled and unfilled red circles, respectively. PS bulk and 18 nm film data shown as filled and unfilled blue squares. Arrows indicate a shift in the film T_g from bulk. (B) ΔT_g versus free-standing film thickness for PMMA and PS shown as red circles and blue squares, respectively. (C) Local α-relaxation time normalized by the bulk-like interior region ($\tau_\alpha/\tau_\alpha^{bulk}$) as a function of film location z for PMMA and PS shown as red circles and blue squares, respectively.

match all-atomistic (AA) and experimental bulk T_g at high cooling rates which are maintained throughout the study. Therefore, we mainly investigate whether the cause of relative confinement differences between polymers systems can be

DOI: 10.1021/acsmacrolett.6b00037
ACS Macro Lett. 2016, 5, 481−486

explained by chemistry-specific attributes incorporated into the CG models.

For free-standing thin films, a layered model consisting of a free-surface layer and an interior bulk-like layer is commonly employed in describing the physics of T_g depression.[2,39] We evaluate the local film relaxation time τ_α along the film thickness z, normalized by the bulk-like interior region τ_α^{bulk} at the temperature $T = T_g^{bulk}$ (Figure 2c). A gradient in local relaxation times is observed with enhanced segmental mobility near the free surface for both systems, penetrating several nanometers further into the interior of the film. The relaxation profile can be captured by the function:[10] $\ln(\tau_\alpha(z)/\tau_\alpha^{bulk}) = -A_0 \exp(-z/\lambda)$, where A_0 and λ are fitting constants. The profile of $\tau_\alpha/\tau_\alpha^{bulk}$ shows a larger shift in relaxation time near the surface for PS than for PMMA. In addition, the local relaxation time converges to within 95% of the bulk relaxation time at a depth of ∼6−7 nm and ∼10−11 nm from the free surface for PMMA and PS, respectively. The differences in the length scale where ΔT_g approaches zero as well as the length scale of local relaxation time enhancement can be correlated with the characteristic size of cooperatively rearranging regions ξ(CRR), theorized by Adam and Gibbs to be strongly connected to the behavior of glass-forming systems.[8,40,41] These results suggest that the length scale of cooperative rearrangement arising from the free surface is greater for PS compared to PMMA, as the perturbed chain dynamics persist further into the film for PS. This observation agrees qualitatively with experimental findings of surface dynamics and CRR (ξ_{PMMA}(CRR) ∼ $1/2\xi_{PS}$(CRR)).[42−45]

The differences in PMMA and PS confinement effect can also be described through comparison of the Debye−Waller factor (DWF) $\langle u^2 \rangle$, a dynamic measurement of the local "rattle-space" between adjacent beads at the picosecond time scale. DWF is generally related to the local free volume v_f by $v_f \sim \langle u^2 \rangle^{\alpha/2}$ which plays a key role in the glass-transition behavior.[34,41,46−48] We evaluate the DWF by measuring the mean-squared displacement of CG atoms at ∼10 ps at T = 350 K, which is below the bulk T_g for both systems to ensure beads are in the caged regime.[33] We find that the normalized surface DWF, $\langle u^2 \rangle_{surf}/\langle u^2 \rangle_{bulk}$ is higher for PS (∼1.85) than for PMMA (∼1.35), indicating a greater shift in free volume occurring in the surface region for PS than that of PMMA.

Next, we focus on understanding the possible mechanisms that cause the above observations from the coarse-grained representation of the PS and PMMA models. Hypothesizing that the differences in PS and PMMA T_g-nanoconfinement behaviors arise from different dynamics of backbone and side-chain beads, we characterize the vibrational density of states (VDOS)[49] $\Phi(\omega)$ as a function of frequency ω for the different CG bead types by calculating the discrete Fourier transform of the velocity autocorrelation function (VACF) $\psi(t)$ (detailed description of VDOS is included in the Supporting Information). We observe distinctly opposing behaviors in the VDOS for the two models in regards to CG bead fluctuations of the effective aggregate chemical groups. The PMMA CG vibrational spectrum obtained from Cartesian coordinates of the side-chain bead force center shows a high intensity normal mode occurring at ∼9 THz corresponding to backbone-side-chain bond stretching vibrations (Figure 3). The PS side-chain, however, shows only a minor backbone-side-chain bond stretching peak near ∼16 THz. These peak frequencies correspond qualitatively with the normal mode peak frequencies of AA VDOS peaks of the Cartesian positions

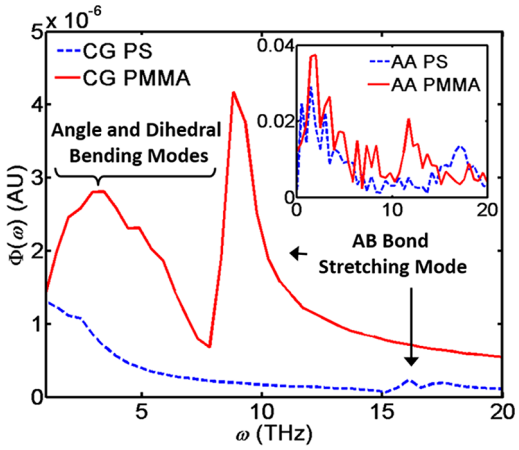

Figure 3. VDOS spectra in arbitrary units for PS and PMMA CG side-chain beads in Cartesian space, as a blue dotted line and red solid line, respectively, indicating larger amplitude side-chain fluctuations in PMMA. (Inset) VDOS spectra for the effective CG bead centers are calculated in the all-atom system for comparison.

of the effective side-group mass centers (Figure 3, inset). The magnitudes of the peaks cannot be compared quantitatively due to other spectral contributions from the additional degrees of freedom in the AA system. This analysis demonstrates that PMMA exhibits characteristically larger amplitude side-chain fluctuations than PS, which suggests greater relative side-chain flexibility for PMMA. This observation of the side-chain flexibility is also consistent with atomistic characteristics where the linear ester side-chain group in PMMA facilitates a higher degree of freedom compared with the rigid phenyl side-chain of PS.

The relative side-chain to backbone mobility is expected to be influenced by the mass distribution within a monomer, which in the case of our 2-bead per monomer coarse-grained models, can be conveniently captured by the backbone to side-chain bead mass ratio m_A/m_B, which is 0.35 for PS and 5.7 for PMMA, respectively. As evident from these values, although the molecular weight of the repeat unit for PS and PMMA is nearly equivalent, the mass is distributed very differently in the two systems. PS has a heavier, more rigid and bulkier phenyl group. In contrast, PMMA has a methyl group attached to the backbone and a more linear and flexible ester side-chain. Considering each monomer is represented as two beads interacting with a spring-like bond, we anticipate that the larger bead should exhibit smaller normal mode fluctuations with respect to the Cartesian frame of reference, and the smaller bead should conversely have larger fluctuations.

On the basis of our VDOS analysis and comparative study of T_g for PS and PMMA, we hypothesize that the side-chain fluctuations can greatly influence the free surface effect on thin film T_g. Specifically, low amplitude side-chain fluctuations associated with lesser side-chain flexibility and lower side-chain-induced free volume facilitate a greater bulk T_g; however, upon free volume introduction in the free-standing film condition, this effect is lost, and a sharp drop in T_g is observed. Using the PS model as a vehicle for parametric study, we vary the mass ratio between the backbone bead (type A) and side-chain bead (type B), m_A/m_B, from 0.1 to 10 while maintaining a constant total mass and thus approximate density. The T_g of bulk and ∼18 nm thick film are then calculated for each mass ratio (Figure 4A). As the mass ratio of the PS model is increased

DOI: 10.1021/acsmacrolett.6b00037
ACS Macro Lett. 2016, 5, 481−486

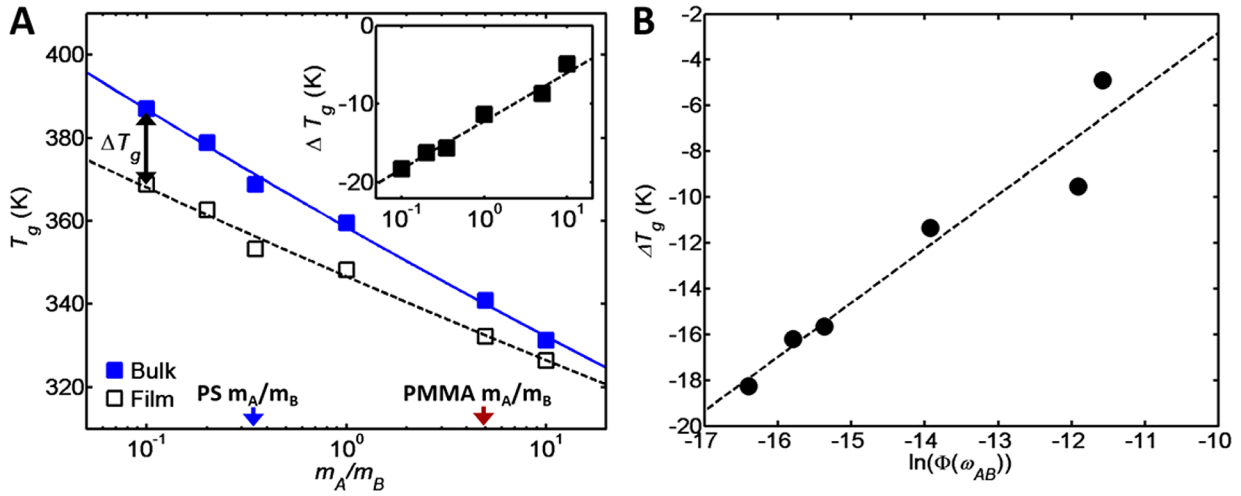

Figure 4. (A) T_g versus backbone to side-chain mass ratio m_A/m_B from systematic parameter changes in the modified PS model. Blue and red arrows show PS and PMMA mass ratio values for reference. (Inset) ΔT_g shows suppressed T_g-confinement effect with increasing mass ratio for the modified PS model. (B) ΔT_g suppression is also correlated with the backbone-side-chain stretching mode peak intensity $\Phi(\omega_{AB})$.

(toward the PMMA mass distribution), we find that the T_g decreases for both bulk and film systems following linear scaling with $\ln(m_A/m_B)$. The general trend of decreasing T_g with increasing side-chain flexibility is similar to the T_g scaling observed in poly(*n*-alkyl methacrylates), where increased polymerization of alkyl chains on the ester side-group lowers the T_g.[3,26] We note that the slightly higher T_g of PMMA compared to PS as seen experimentally is attained by implementing stronger side-chain cohesive interactions in the original CG formulations, which is consistent with higher polarity found in the PMMA ester group. White et al. also observed a higher cohesive energy density for PMMA than PS using polymer-specific empirical lattice models, which they attributed as one potential reason why higher T_g depression for PS free-standing films with decreasing film thickness was observed.[23] The cohesive energy density appears to play a key role in T_g-nanoconfinement in combination with other structural factors;[50] however, when only varying cohesive interactions of either backbone or side-chain beads (ε_{AA} = 0.1−0.5 kcal/mol, ε_{BB} = 0.3−1.4 kcal/mol), we do not find a consistent trend in ΔT_g for our 2-bead CG models.

In addition, ΔT_g is suppressed for larger mass ratios, as shown in Figure 4A inset, and scales linearly with $\ln(m_A/m_B)$. At the mass ratio pertinent to PS (m_A/m_B = 0.35), ΔT_g is ∼−17 K. After modifying the mass ratio to the equivalent distribution for PMMA (m_A/m_B = 5.7), the ΔT_g shifts to ∼−8 K, indicating reduced free surface effect. This may be explained through the following reasoning: For increasing mass ratio, the lighter side-chain group undergoes higher amplitude oscillations in Cartesian space, thus exhibiting greater side-chain flexibility and higher side-chain contribution to free volume around the chain. The CRR size has been shown to decrease with increasing free volume,[41] which leads to diminished mobility propagation into the film interior and suppresses T_g-nanoconfinement effect. We acknowledge, however, that differences in the CRR size may not be the only factor explaining the dissimilarity in the free surface effect for PS and PMMA. The VDOS peak intensity $\Phi(\omega_{AB})$ for the normal-mode frequency ω_{AB} associated with backbone to side-chain bond vibrations is measured at each mass ratio condition (Figure S2). We find that ΔT_g scales linearly with $\ln(\Phi(\omega_{AB}))$, showing a connection between ΔT_g and the side-chain fluctuation amplitude in Cartesian space, as shown in Figure 4B. The fragility m defined as $m = [d(\log \tau_\alpha)/d(T_g/T)]_{T=T_g}$ is also computed for the bulk systems and is found to be statistically invariable for different mass ratios. This allows us to rule out fragility in the bulk as a predictor of nanoconfinement differences between PS and PMMA, confirmed by the similar experimental fragility measurements for PS (103−145) and PMMA (116−143).[19]

A similar trend of decreasing T_g-nanoconfinement effect with increasing backbone to side-chain mass ratio can be seen from experimental comparisons of PS, poly(α-methylstyrene) (PαMS), poly(4-methylstyrene) (P4MS), and poly(*tert*-butylstyrene) (PTBS) supported films.[1,25,51] PαMS contains a methyl group at the backbone α-carbon, which effectively increases the backbone to side-chain mass ratio and causes a reduced T_g-nanoconfinement effect in 20 nm films ($\Delta T_g^{P\alpha MS}$ = −12 K) compared to PS (ΔT_g^{PS} = −17 K). When the methyl group is added instead, to the para 4-position on the phenyl side-group in P4MS, effectively decreasing the mass ratio, the T_g-nanoconfinement effect increases (ΔT_g^{P4MS} = −33 K). Furthermore, addition of a heavier *tert*-butyl group to the para position of the benzene ring produces a much greater T_g depression (ΔT_g^{PTBS} = −47 K). We note that CRR size, however, was not found to correlate with mass ratio in this case, and therefore, the length scale of cooperative motion is not the only factor influencing the differences in T_g-nanoconfinement effect for these systems. In addition, the strength of the free surface effect with mass ratio appears to hold especially for bulky side groups, as mass added to the side-group of PMMA through relatively linear alkyl polymerization has the opposite effect on T_g-nanoconfinement.[26] We suggest that this is because linear alkyl polymerization of PMMA increases side-chain flexibility and generates greater free volume, which has a similar effect as increasing the mass ratio. Examining the effects of adding a linear side-group consisting of a chain of beads using our CG model could provide a more direct comparison for this case.

In summary, our simulation results for PS and PMMA CG models show that the reduced T_g-nanoconfinement effect in PMMA compared to PS can be attributed to increased side-chain flexibility associated with chemical structure features such as mass distribution and side-chain fluctuations. Our results

DOI: 10.1021/acsmacrolett.6b00037
ACS Macro Lett. 2016, 5, 481−486

suggest that the bulky, rigid phenyl side-group in PS is responsible for a high T_g in the bulk, larger characteristic size for cooperativity and enhanced relaxation region length scale, but upon free volume introduction in the free-standing film condition, a larger T_g shift and therefore greater T_g-nanoconfinement effect is produced. In contrast, the higher side-chain flexibility in PMMA is responsible for decreased characteristic size for cooperativity and higher side-group induced free volume. Consequently, the propagation of free surface induced chain mobility into the film is diminished in PMMA compared to PS. Our findings elucidate the possible molecular origins of unexplained phenomena as observed in nanoscale polymer thin films and highlight the predictive power of chemistry-specific CG modeling for providing insight toward the physics of polymer systems.

■ ASSOCIATED CONTENT

Supporting Information

The Supporting Information is available free of charge on the ACS Publications website at DOI: 10.1021/acsmacrolett.6b00037.

Additional information on general simulation methodology, procedure for estimating structural relaxation time and glass transition temperature, method for calculating the vibrational density of states, and parameters of the coarse-grained models (PDF)

■ AUTHOR INFORMATION

Corresponding Author

*Tel.: 847-491-5282. E-mail: s-keten@northwestern.edu.

Author Contributions

‖These authors contributed equally to this work.

Notes

The authors declare no competing financial interest.

■ ACKNOWLEDGMENTS

D.H., W.X., J.S., and S.K. acknowledge support by the University Partnership Initiative between Northwestern University and The Dow Chemical Company and from the Dept. of Civil & Environmental Engineering and Mechanical Engineering at Northwestern University. The authors acknowledge valuable discussions with John Torkelson, Linda Broadbelt and Steven Arturo. A supercomputing grant from Quest HPC System at Northwestern University is also acknowledged.

■ REFERENCES

(1) Keddie, J. L.; Jones, R. A.; Cory, R. A. *Europhys. Lett.* **1994**, *27*, 59.
(2) Ediger, M.; Forrest, J. *Macromolecules* **2013**, *47*, 471−478.
(3) Priestley, R. D.; Mundra, M. K.; Barnett, N. J.; Broadbelt, L. J.; Torkelson, J. M. *Aust. J. Chem.* **2007**, *60*, 765−771.
(4) Roth, C. B.; Dutcher, J. R. *J. Electroanal. Chem.* **2005**, *584*, 13−22.
(5) Alcoutlabi, M.; McKenna, G. B. *J. Phys.: Condens. Matter* **2005**, *17*, R461.
(6) Qin, X.; Xia, W.; Sinko, R.; Keten, S. *Nano Lett.* **2015**, *15*, 6738−6744.
(7) Hanakata, P. Z.; Douglas, J. F.; Starr, F. W. *Nat. Commun.* **2014**, *5*, 5.
(8) Lang, R. J.; Simmons, D. S. *Macromolecules* **2013**, *46*, 9818−9825.
(9) Peter, S.; Meyer, H.; Baschnagel, J.; Seemann, R. *J. Phys.: Condens. Matter* **2007**, *19*, 205119.
(10) Peter, S.; Meyer, H.; Baschnagel, J. *J. Polym. Sci., Part B: Polym. Phys.* **2006**, *44*, 2951−2967.
(11) Xia, W.; Keten, S. *J. Mater. Res.* **2015**, *30*, 36−45.
(12) Xia, W.; Keten, S. *Extreme Mech. Lett.* **2015**, *4*, 89−95.
(13) Torres, J. M.; Stafford, C. M.; Vogt, B. D. *ACS Nano* **2009**, *3*, 2677−2685.
(14) Wang, J.; McKenna, G. B. *Macromolecules* **2013**, *46*, 2485−2495.
(15) Forrest, J.; Dalnoki-Veress, K.; Stevens, J.; Dutcher, J. *Phys. Rev. Lett.* **1996**, *77*, 2002.
(16) Ellison, C. J.; Torkelson, J. M. *Nat. Mater.* **2003**, *2*, 695−700.
(17) Roth, C. B.; Dutcher, J. *Eur. Phys. J. E: Soft Matter Biol. Phys.* **2003**, *12*, 103−107.
(18) Harper, C. A.; Baker, A.-M. *Modern Plastics Handbook*; McGraw-Hill: New York, 2000.
(19) Kunal, K.; Robertson, C. G.; Pawlus, S.; Hahn, S. F.; Sokolov, A. P. *Macromolecules* **2008**, *41*, 7232−7238.
(20) Mark, J. E. *Physical Properties of Polymers Handbook*; Springer: 2007; Vol. *1076*.
(21) Rubinstein, M.; Colby, R. H. *Polymer Physics*; OUP: Oxford, 2003.
(22) Roth, C.; Pound, A.; Kamp, S.; Murray, C.; Dutcher, J. *Eur. Phys. J. E: Soft Matter Biol. Phys.* **2006**, *20*, 441−448.
(23) White, R. P.; Price, C. C.; Lipson, J. E. *Macromolecules* **2015**, *48*, 4132−4141.
(24) Ellison, C. J.; Ruszkowski, R. L.; Fredin, N. J.; Torkelson, J. M. *Phys. Rev. Lett.* **2004**, *92*, 095702.
(25) Ellison, C. J.; Mundra, M. K.; Torkelson, J. M. *Macromolecules* **2005**, *38*, 1767−1778.
(26) Campbell, C. G.; Vogt, B. D. *Polymer* **2007**, *48*, 7169−7175.
(27) Shavit, A.; Riggleman, R. A. *Macromolecules* **2013**, *46*, 5044−5052.
(28) Xie, S.-J.; Qian, H.-J.; Lu, Z.-Y. *J. Chem. Phys.* **2015**, *142*, 074902.
(29) Evans, C. M.; Deng, H.; Jager, W. F.; Torkelson, J. M. *Macromolecules* **2013**, *46*, 6091−6103.
(30) Lan, T.; Torkelson, J. M. *Macromolecules* **2016**, *49*, 1331−1343.
(31) Hsu, D. D.; Xia, W.; Arturo, S. G.; Keten, S. *J. Chem. Theory Comput.* **2014**, *10*, 2514−2527.
(32) Hsu, D. D.; Xia, W.; Arturo, S. G.; Keten, S. *Macromolecules* **2015**.
(33) Xia, W.; Hsu, D. D.; Keten, S. *Macromol. Rapid Commun.* **2015**, *36*, 1422−1427.
(34) Simmons, D. S.; Cicerone, M. T.; Zhong, Q.; Tyagi, M.; Douglas, J. F. *Soft Matter* **2012**, *8*, 11455−11461.
(35) Mangalara, J. H.; Simmons, D. S. *ACS Macro Lett.* **2015**, *4*, 1134−1138.
(36) Baschnagel, J.; Binder, K.; Doruker, P.; Gusev, A. A.; Hahn, O.; Kremer, K.; Mattice, W. L.; Muller-Plathe, F.; Murat, M.; Paul, W.; Santos, S.; Suter, U. W.; Tries, V. *Adv. Polym. Sci.* **2000**, *152*, 41−156.
(37) Fakhraai, Z.; Forrest, J. A. *Phys. Rev. Lett.* **2005**, *95*, 025701.
(38) Baljon, A.; Williams, S.; Balabaev, N.; Paans, F.; Hudzinskyy, D.; Lyulin, A. *J. Polym. Sci., Part B: Polym. Phys.* **2010**, *48*, 1160−1167.
(39) Forrest, J. A.; Mattsson, J. *Phys. Rev. E: Stat. Phys., Plasmas, Fluids, Relat. Interdiscip. Top.* **2000**, *61*, R53.
(40) Adam, G.; Gibbs, J. H. *J. Chem. Phys.* **1965**, *43*, 139−146.
(41) Betancourt, B. A. P.; Hanakata, P. Z.; Starr, F. W.; Douglas, J. F. *Proc. Natl. Acad. Sci. U. S. A.* **2015**, *112*, 2966−2971.
(42) Dalnoki-Veress, K.; Forrest, J.; De Gennes, P.; Dutcher, J. *J. Phys. IV* **2000**, *10*, Pr7−221−Pr7−226.
(43) Sharp, J.; Forrest, J. *Eur. Phys. J. E: Soft Matter Biol. Phys.* **2003**, *12*, 97−101.
(44) Paeng, K.; Ediger, M. *Macromolecules* **2011**, *44*, 7034−7042.
(45) Paeng, K.; Swallen, S. F.; Ediger, M. *J. Am. Chem. Soc.* **2011**, *133*, 8444−8447.
(46) Widmer-Cooper, A.; Harrowell, P. *Phys. Rev. Lett.* **2006**, *96*, 185701.
(47) Starr, F. W.; Sastry, S.; Douglas, J. F.; Glotzer, S. C. *Phys. Rev. Lett.* **2002**, *89*, 125501.
(48) Napolitano, S.; Rotella, C.; Wübbenhorst, M. *ACS Macro Lett.* **2012**, *1*, 1189−1193.
(49) Shuker, R.; Gammon, R. W. *Phys. Rev. Lett.* **1970**, *25*, 222.
(50) Xu, W.-S.; Freed, K. F. *Macromolecules* **2014**, *47*, 6990−6997.

DOI: 10.1021/acsmacrolett.6b00037
ACS Macro Lett. 2016, 5, 481−486

(51) Kim, J. H.; Jang, J.; Zin, W.-C. *Langmuir* **2001**, *17*, 2703−2710.

DOI: 10.1021/acsmacrolett.6b00037
ACS Macro Lett. 2016, 5, 481−486